BIOCHEMISTRY
including biophysical chemistry & molecular biology

Article

pubs.acs.org/biochemistry

Interfacial Activation of *Candida antarctica* Lipase B: Combined Evidence from Experiment and Simulation

Themistoklis Zisis,[†] Peter L. Freddolino,[‡] Petri Turunen,[†] Muriel C. F. van Teeseling,[†,#] Alan E. Rowan,*[,†] and Kerstin G. Blank*[,†]

[†]Institute for Molecules and Materials, Radboud University, Department of Molecular Materials, Heyendaalseweg 135, 6525 AJ Nijmegen, The Netherlands

[‡]Department of Biological Chemistry, University of Michigan Medical School, Ann Arbor, Michigan 48109, United States

Supporting Information

ABSTRACT: Lipase immobilization is frequently used for altering the catalytic properties of these industrially used enzymes. Many lipases bind strongly to hydrophobic surfaces where they undergo interfacial activation. *Candida antarctica* lipase B (CalB), one of the most commonly used biocatalysts, is frequently discussed as an atypical lipase lacking interfacial activation. Here we show that CalB displays an enhanced catalytic rate for large, bulky substrates when adsorbed to a hydrophobic interface composed of densely packed alkyl chains. We attribute this increased activity of more than 7-fold to a conformational change that yields a more open active site. This hypothesis is supported by molecular dynamics simulations that show a high mobility for a small "lid" (helix α5) close to the active site. Molecular docking calculations confirm that a highly open conformation of this helix is required for binding large, bulky substrates and that this conformation is favored in a hydrophobic environment. Taken together, our combined approach provides clear evidence for the interfacial activation of CalB on highly hydrophobic surfaces. In contrast to other lipases, however, the conformational change only affects large, bulky substrates, leading to the conclusion that CalB acts like an esterase for small substrates and as a lipase for substrates with large alcohol substituents.

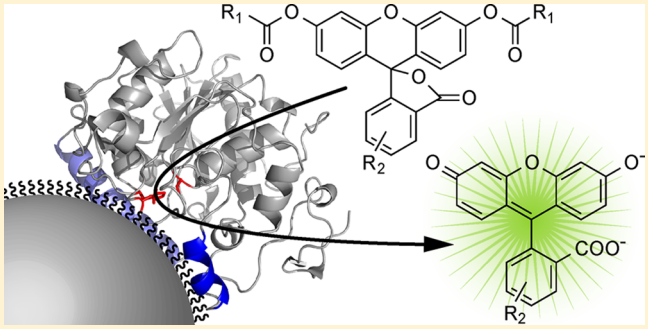

Esterases and lipases are ubiquitous enzymes that are found in all kingdoms of life. Both esterases (EC 3.1.1.1) and lipases (EC 3.1.1.3) hydrolyze ester bonds between alcohols and carboxylic acids, but with different substrate specificity. Whereas esterases act on water-soluble substrates containing short-chain carboxylic acids, lipases prefer to hydrolyze triglycerides with long-chain fatty acids that are not water-soluble and aggregate in aqueous solution.[1−4] In contrast to esterases, lipases typically appear in two main conformations: a closed and an open conformation. In the closed conformation, an amphiphilic α-helix, the so-called lid, secludes the active site from the medium. The open form is characterized by lid displacement and exposure of the hydrophobic residues around the active site to the medium.[1−3,5,6] The exposure of this large hydrophobic area is energetically unfavorable in the absence of a hydrophobic interface, leading to stabilization of the closed conformation. Upon binding to the oil−water interface, the lid opens and the exposed hydrophobic surface area contributes to the interaction between the enzyme and its substrate.

Despite this important structural difference between lipases and esterases, both can accommodate a broad range of substrates with varying substituents on the alcohol and the carboxylic acid. This broad specificity, combined with a high enantio- and regioselectivity, has made these enzymes useful in a wide range of industrial applications.[4,7,8] Many lipases are stable in organic solvents where they can be used for catalyzing ester bond formation or transesterification reactions.[3,4,8] *Candida antarctica* lipase B (CalB),[9,10] recently reclassified as *Pseudozyma antartica* lipase B (PalB),[11] is a commonly used industrial enzyme with a very broad substrate specificity. It is highly active toward a broad range of esters, thiols, and amides, but less active toward large triglycerides.[12]

From a structural point of view, CalB is a typical lipase. It is a member of the α/β-hydrolase fold family with a Ser-Asp-His catalytic triad.[9] It contains two mobile α-helices surrounding the active site (α5 and α10) that contribute to the ability of the enzyme to accommodate many different substrates.[13] Many experimental and simulation studies have been performed to understand and tune the catalytic activity of CalB. In a number of studies it has been shown that physical adsorption is a powerful method to alter the stability, activity, and even enantioselectivity of CalB.[14−16] Early molecular docking studies provided insight into the structural basis of CalB substrate specificity including its enantioselectivity.[10,17,18] The insight

Received: May 30, 2015
Revised: August 28, 2015
Published: September 8, 2015

DOI: 10.1021/acs.biochem.5b00586
Biochemistry 2015, 54, 5969−5979

provided by these studies has allowed a detailed dissection of the thermodynamic contributions to the chiral resolution for a variety of substrates.[18] More importantly, it has enabled the rational redesign of the CalB active site with the goal of altering its substrate specificity.[19−22]

More recently, attention has turned from engineering the substrate binding site to studying the overall dynamics of CalB with a special focus on the α5 and α10 helices that surround most of the active site. Lid swapping of the α5 helix with lid domains of other lipases has revealed a crucial role of the α5 helix in substrate specificity and enantioselectivity.[13] Circular permutation experiments have shown that the N- and C-termini can be relocated into the α10 helix with a dramatic effect on CalB activity.[23,24] Also mechanical force has been shown to alter CalB activity most likely by inducing structural changes around the α10 helix.[25] In agreement with these experimental observations, several molecular dynamics studies have shown the important role of the α5 and α10 helices for CalB activity, highlighting that these helices are the most mobile parts of the structure.[13,26−28] In a particularly elegant series of simulations, Pleiss and co-workers[27] have shown that, upon coming into close proximity with a hydrophobic interface, CalB is initially anchored in the bilayer by burial of the α5 helix into the hydrophobic layer. Subsequently, the enzyme reorients and binds to the interface, appropriately positioning its active site. Independently, Skjøt and colleagues used a short (10 ns) molecular dynamics simulation to illustrate the possibility that the α5 helix could act as a lid, observing motion of α5 toward α10. These simulations highlight the crucial role of the α5 helix for establishing the interaction of CalB with hydrophobic interfaces, but do not provide unambiguous proof that α5 has a lid-like function.[7,13]

Despite this huge progress in understanding and controlling the catalytic activity of CalB, the presence of a lid structure is discussed controversially, and clear experimental evidence for interfacial activation of CalB is still lacking.[7,27,29−31] In this paper we show that CalB is an interfacially activated enzyme and that activation depends both on the hydrophobicity of the interface as well as the overall size of the substrate. In a series of systematic experiments, we have immobilized CalB on a number of supports with varying degrees of hydrophobicity via physical adsorption. Using these preparations of immobilized CalB, we have performed activity measurements using chromogenic and fluorogenic substrates of different sizes. To test for possible interfacial activation caused by the hydrophobic surface, we have performed these measurements in aqueous conditions that normally favor the lid-closed conformation of typical lipases. We have further performed extensive simulations to gain structural insight into the conformational states of CalB when interacting with surfaces of different hydrophobicity and binding to different substrates. Using a combination of atomistic-resolution simulation, coarse-grained modeling, and docking calculations, we have obtained a comprehensive energetic picture of the interplay between enzyme conformation, surface hydrophobicity, and substrate specificity.

EXPERIMENTAL PROCEDURES

Materials. Unless otherwise stated, all chemicals were purchased from Sigma-Aldrich or VWR and used without further purification. The substrates 5,6-carboxyfluorescein diacetate (CFDA) and fluorescein dibutyrate (FDB) were obtained from Chemodex. Fluorescein diacetate (FDA) was purchased from LifeTechnologies. The suicide inhibitor methyl-4-methyl-umbelliferyl hexylphosphonate (ELSI-MF) was obtained from Eucodis Bioscience GmbH. The PEG-terminated silane (2-[methoxy (polyethyleneoxy)$_{21-24}$ propyl] trimethoxysilane) was obtained from ABCR. Prior to silanization, the silanes (trimethoxy methyl silane, trimethoxy propyl silane, trimethoxy octyl silane, trimethoxy octadecyl silane) as well as the PEG-terminated silane were distilled, aliquoted in glass vials, and stored under oxygen free and dry conditions.

Silanization of Glass Beads. Glass beads (1 μm diameter; Bangs Laboratories, Inc.) were suspended in ultrapure water (2 g/mL). To generate additional silanol groups on the surface, they were treated with Piranha solution (H_2SO_4/H_2O_2 3:1; CAUTION: Piranha solution is highly corrosive and an extremely powerful oxidizer; prepare in a ventilated area). The bead suspension (200 μL) was added to 10 mL of the Piranha solution in a glass test tube and stirred gently for 30 min. The sample was centrifuged at 4000 rpm for 10 min. After the supernatant was removed, the beads were washed with 3 × 10 mL ultrapure water. Subsequently, the silane solution was added to the test tube. The silane solution contained 0.6 mM of the respective silane dissolved in a mixture of 10% ultrapure water and 90% ethanol (spectrophotometry grade). The suspension was stirred gently for 48 h at room temperature. After centrifugation at 4000 rpm for 10 min, the supernatant was removed and the beads were sonicated 3× for 5 min with isopropanol (spectrophotometry grade). Subsequently, they were dried under a stream of nitrogen and stored in an oxygen free and dark environment.

Enzyme Immobilization on Silanized Beads. CalB labeled with ATTO565 (see Supporting Information (SI) for details) was diluted to a concentration of 2.5 μM (5× the final concentration) in activity buffer (50 mM NaH_2PO_4 pH 7.0, 150 mM NaCl). The enzyme solution (20 μL) was incubated with an excess of silanized beads (0.22 mg) for approximately 30 min on ice. The beads were used for the following activity measurements without washing as no residual enzymes were detected in the supernatant after this 30 min incubation time (see SI for details).

Active-Site Titration. The amount of active CalB enzymes in the enzyme preparation was determined using the suicide inhibitor methyl-4-methyl-umbelliferyl hexylphosphonate (ELSI-MF). The inhibitor was dissolved in dry DMSO at a concentration of 50 μM. The measurement was performed with an enzyme concentration of 500 nM and an inhibitor concentration of 5 μM. To prepare the samples, 20 μL of 2.5 μM CalB was premixed with 70 μL of 1× activity buffer in a black, flat-bottom 96-well plate (BD Falcon). Alternatively, 20 μL of a bead suspension was used carrying the same amount of immobilized CalB. To start the measurement, 10 μL of the inhibitor was added, yielding a final DMSO concentration of 10%. Subsequently, each well was covered with 50 μL of mineral oil to prevent evaporation. The release of the fluorophore 7-hydroxy-4-methylcoumarin was followed in a microplate reader (λ_{ex} = 365 nm; λ_{em} = 460 nm; Tecan Infinite M200 PRO). The measurement was performed at 25 °C for 15 min (30 s intervals). All measurements were performed in triplicate. The detected fluorescence signal was converted into the actual product concentration using a calibration curve of the product 7-hydroxy-4-methylcoumarin and subsequently corrected for autohydrolysis of ELSI-MF. As every active enzyme performs exactly one enzymatic turnover, during the measure-

DOI: 10.1021/acs.biochem.5b00586
Biochemistry 2015, 54, 5969−5979

ment time, the final product concentration directly corresponds to the concentration of active sites.

Activity Measurements Using the Chromogenic Substrate *p*NPB. All measurements using the substrate *para*-nitrophenol butyrate (*p*NPB) were carried out with a substrate concentration of 100 μM and an enzyme concentration of 500 nM. Prior to the measurement the substrate was diluted to a concentration of 2 mM in dry DMSO. The measured samples contained 10 μL of 2 mM substrate, 150 μL of 1× activity buffer and 40 μL of 2.5 μM CalB immobilized on the silanized glass beads (200 μL final volume with 5% DMSO). Beads and buffer were premixed in the cuvette, and substrate was added just before the measurement. The measurement was performed in disposable polystyrene cuvettes, following absorbance at 405 nm using an UV/vis spectrometer (VARIAN Cary300). The samples were measured at 25 °C for approximately 30 min (30 s intervals). All measurements were performed in triplicate.

Activity Measurements Using Fluorogenic Substrates. The fluorogenic substrates FDA, CFDA, and FDB were used for measuring the activity of immobilized CalB. All substrates were dissolved in dry DMSO at a concentration of 100 μM. The activity was measured using a substrate concentration of 10 μM and an enzyme concentration of 500 nM. The measured samples contained 10 μL of 100 μM substrate, 70 μL of 1× activity buffer, and 20 μL of 2.5 μM of CalB immobilized on the silanized glass beads (100 μL final volume with 10% DMSO). Beads and buffer were premixed in the well plate, and substrate was added just before the measurement. Finally, each well containing a sample was covered with 50 μL of mineral oil to prevent evaporation. The release of the fluorophores fluorescein or 5,6-carboxyfluorescein was followed in the microplate reader (λ_{ex} = 495 nm; λ_{em} = 525 nm). The measurement was performed at 25 °C for 48 h (30 s intervals). All measurements were performed in triplicate. The turnover rate was calculated for the first reaction step (conversion of the double-substituted substrate into the weakly fluorescent intermediate). The data were corrected for autohydrolysis of the substrate and the concentration of active sites. Details of the calculations are described in the SI.

Molecular Dynamics Simulations and Analysis. All molecular dynamics simulations were performed using NAMD 2.6.[32] The CHARMM22 force field with CMAP corrections[33,34] was used for the protein, and the TIP3P water model[35] for water. The temperature of each replica was maintained using Langevin dynamics with a damping constant of 5.0 ps^{-1}. Short-range interactions were cut off at 1.2 nm, with switching starting at 1.0 nm. Long-range electrostatics were treated using the Particle Mesh Ewald method[32] with a grid density no lower than 1 per angstrom. Dynamics were propagated using a 2.0 fs time step, with nonbonded interactions evaluated every step and long-range electrostatics every other step. The initial structure was generated by taking the protein component of PDB code 1TCA, with water and ions (0.154 M NaCl was sufficient to neutralize the system) added using VMD.[36] The system was minimized for 3000 steps, subjected to 10 ps of equilibration with the protein fixed and then 100 ps of equilibration with the protein mobile.

After equilibration, parallel tempering simulations[37] were initiated with 48 replicas, with temperatures ranging from 300 to 400 K. Temperature exchanges were attempted once per picosecond. Temperature spacing of the replicas was optimized to yield average exchange frequencies between 30% and 40%. Each replica was run for 21 ns for a total run time of 1.008 μs, with snapshots saved for subsequent analysis once every 10 ps.

Dominant conformations from the replica exchange trajectories (subsequently used for the docking calculations) were identified using the g_cluster module of GROMACS 3.3.3.[38] All frames were first aligned using all nonsymmetry-related heavy atoms from the main β-sheet and then clustered using the Gromos method[39] with a 0.15 nm cutoff, considering only residues of the α5 helix (residues 142−146) and the C-terminal portion of the α10 helix (residues 278−287). For the docking calculations the 24 most occupied clusters were considered, which collectively represent more than 95% of all time steps.

As motion of the α5 helix over the active site is a dominant contributor to the observed dynamics of the protein, the α5-α10 cleft distance is used a metric describing active site accessibility. This distance is defined as the center of mass distance between residues 142−145 (α5) and residues 278−287 (C-terminal half of α10). For simplicity of interpretation the different conformations were partitioned into three classes: closed (α5-α10 cleft distance less than 1.52 nm), crystal-like (cleft distance 1.52—1.90 nm), and open (cleft distance greater than 1.90 nm). For comparison, the α5-α10 cleft distance is 1.63 nm in the starting crystal structure and 1.71 nm in the most heavily occupied conformation from molecular dynamics simulations.

Docking Calculations. Docking was used to identify the preferred conformations and approximate binding affinities of the experimentally used substrates (Figure S1). For the substrate 5,6-CFDA, the isomers 5-CFDA and 6-CFDA were docked separately. For docking, each of the cluster-representative conformations were used, as well as the MD-equilibrated structure and the 1LBS crystal structure (which was crystallized with an inhibitor bound and thus is more likely to represent an active-like conformation).

The structures were prepared for docking using UCSF Chimera 1.7.[40] The hydrogen atoms were placed to optimize hydrogen bonding (with the key histidine residue H224 constrained to delta protonation only) and AMBER ff12SB charges were used for all residues. All substrates (Figure S1) were prepared for docking using the antechamber plugin of Chimera 1.7. Structures were minimized with 1000 steepest descent steps of AM1 geometry optimization and then charged using AM1-BCC charges. All docking calculations were performed with UCSF DOCK version 6.1,[41] using SYBYL atom types.

For the initial round of docking a grid-based scoring was used, generating up to 32 000 docked poses per ligand-protein structure combination; these settings were identified based on pilot calculations showing that this level of search effort would prove saturating for our largest ligands. While holding the protein fixed, the simulations allowed simplex minimization of both anchor poses and final ligand poses. During docking, poses were clustered with a 0.1 nm RMSD cutoff after minimization and only one representative for each cluster retained. After docking, conformations were filtered to retain only those in which the S105 catalytic oxygen was within 0.6 nm of the substrate ester carbon. Binding energies reflect the minimized dock scores for these representative minimized conformations.

Conformational Free Energy Estimates. The occupancies of different clustered conformations in solution were estimated using the multistate Bennett acceptance ratio

DOI: 10.1021/acs.biochem.5b00586
Biochemistry 2015, 54, 5969−5979

(MBAR),[42] as implemented in pymbar 2.1.0beta. First, all trajectory frames were rebinned into the top 24 clustered conformations based on the conformation of the gateway helices (as described above), discarding the first 6 ns of each trajectory. Using this clustering assignment, the mean dwell time in all but two clusters was less than 10 frames (100 ps). The trajectories were subsampled to take only every 10th frame in the MBAR analysis, then treating the resulting trajectories as uncorrelated. Occupancies and corresponding uncertainties were then estimated at 308 K using the computeExpectations function of pymbar.[42]

The effects of a hydrophobic interface on the conformational free energies were estimated using a simple continuum solvent model. The experimental setup was considered to consist of an impenetrable slab, a slab of hydrophobic material with variable thickness, and an infinite layer of aqueous solvent. The amino acids were divided into five classes. Each class is characterized by an approximate free energy for transfer between aqueous solvent and the hydrophobic layer (Table 1). Using these free energies, the partition weight for each protein conformation to be transferred into a hydrophobic layer of given thickness was calculated. It was obtained by summing over a three-dimensional grid of all possible protein orientations (θ and φ, at 2 deg increments) and distances from the bead surface (z, at 0.2 Å increments). The distances were chosen to range from the closest possible approach without intersecting the impermeable slab (bead) to the point where all protein atoms have lost contact with the hydrophobic layer. The occupancy of each conformation, assuming contact with the hydrophobic layer, was then estimated by reweighting the bulk solvent occupancies of each conformation by the summed partition weights of all orientations of that conformation interacting with the hydrophobic bead layer obtained using the coarse model above.

Table 1. Parameters Used for the Approximate Hydrophobic Interface Interaction Model[a]

class	residue types	$dG_{water \rightarrow slab}$ (kcal/mol A^2)[b]
1	L, I, V	−0.027
2	F, M, W, A, C, G	−0.013
3	Y	0
4	T, S, H, Q, K	0.026
5	N, E, D, R	0.051

[a]Each residue type contributes to the estimated free energy based on its solvent accessible surface area (SASA) exposed to the hydrophobic slab. [b]Based on experimental data from Radzicka et al.[43] N.b. only SASA of side chain atoms contributes to the free energy change.

RESULTS

Experimental Design. Recombinant CalB, expressed in *Escherichia coli*[44,45] (see SI for details), was incubated with silanized glass beads of different hydrophobicity (Figure 1). More precisely, the beads were modified with methyl- propyl- octyl- or octadecyl-terminated silanes to produce well-defined and highly packed hydrophobic self-assembled silane monolayers (SAMs). A silane with a hydrophilic poly(ethylene glycol) chain was used as a control. After physisorption of CalB to the silanized beads, CalB activity was measured using the water-soluble chromogenic substrate *para*-nitrophenol butyrate (*p*NPB, **1**) or one of the fluorogenic substrates fluorescein diacetate (FDA, **2**) 5,6-carboxyfluorescein diacetate (CFDA, **3**) and fluorescein dibutyrate (FDB, **4**). For all these substrates, the enzymatic reaction yields a colored (**1**) or fluorescent (**2**–**4**) product that can easily be measured spectroscopically (Figure 1, Figure S1).

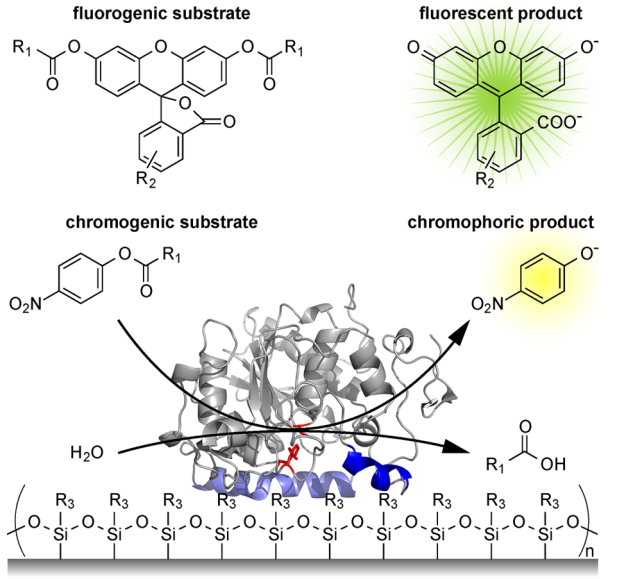

Figure 1. Experimental design showing the different fluorogenic and chromogenic substrates used for measuring CalB activity: *p*NPB (**1**; $R_1 = (CH_2)_2CH_3$), FDA (**2**; $R_1 = CH_3$, $R_2 = H$), 5,6-CFDA (**3**; $R_1 = CH_3$, $R_2 = COOH$), FDB (**4**, $R_1 = (CH_2)_2CH_3$, $R_2 = H$). CalB is immobilized noncovalently on SAM surfaces of different hydrophobicity: PEG-terminated SAM $R_3 = (EG)_{21-24}$, methyl-terminated SAM $R_3 = CH_3$, propyl-terminated SAM $R_3 = (CH_2)_2CH_3$, octyl-terminated SAM $R_3 = (CH_2)_7CH_3$, octadecyl-terminated SAM $R_3 = (CH_2)_{17}CH_3$.

Surface Preparation and Characterization. The silanization protocol using trimethoxysilanes was first tested on glass coverslips to ensure that indeed monolayers were formed. Water contact angle measurements of the resulting surfaces show a range between 49.7° for trimethoxy methylsilane and 89.9° for trimethoxy octylsilane (Table 2 and SI). The contact angle increases with increasing alkyl chain length, clearly showing that the surface hydrophobicity can be tuned by varying the length of the alkyl chain. Atomic force microscopy (AFM) measurements were used to obtain information about the thickness and the homogeneity of the silane layer. The layer thickness was determined to be 0.8 and 1.5 nm for the trimethoxy propylsilane and the trimethoxy octlysilane functionalized glass coverslips, respectively (Figure S4). These values correspond well to the theoretical thickness of 0.9 nm for a propyl-terminated and 1.6 nm for an octyl-terminated monolayer.

Enzyme Immobilization. For the activity measurements CalB was immobilized on glass beads silanized using exactly the same protocol as for the glass coverslips. Before activity measurements were performed, the immobilization efficiency was tested first. ATTO565-labeled CalB was mixed with the glass beads and incubated for 30 min. Subsequently, the beads were separated from the solution, and the fluorescence intensity of the supernatant was determined. The remaining fluorescence in the supernatant was less than 6% for all surfaces tested (Table 2). Also only very little enzymatic activity was detected in the supernatant when adding the substrate FDB (see SI for details). Taken together, these results show that CalB binds

DOI: 10.1021/acs.biochem.5b00586
Biochemistry 2015, 54, 5969−5979

Table 2. Enzyme Immobilization on Surfaces of Different Hydrophobicity

	PEG	methyl	propyl	octyl	octadecyl
contact angle (deg)	37.1 ± 0.6	49.7 ± 0.8	64.2 ± 1.1	89.9 ± 1.0	n.d.[a]
immobilized enzymes (%)	94.3 ± 0.3	96.2 ± 0.6	95.6 ± 0.7	96.3 ± 0.6	97.0 ± 0.6
active enzymes (%)	54.2 ± 7.8	62.3 ± 12.2	68.0 ± 14.1	69.5 ± 9.3	59.7 ± 11.5

[a]n.d. − not determined.

Table 3. Enzymatic Turnover Rate on Surfaces of Different Hydrophobicity (1/s)

	free CalB	PEG	methyl	propyl	octyl	octadecyl
*p*NPB	0.80 ± 0.05	0.54 ± 0.09	0.65 ± 0.18	0.67 ± 0.27	0.59 ± 0.15	0.91 ± 0.27
FDA	0.0104 ± 0.0055	0.0138 ± 0.0061	0.0138 ± 0.0053	0.0118 ± 0.0052	0.0191 ± 0.0085	0.0494 ± 0.0269
CFDA	0.0086 ± 0.0017	0.0065 ± 0.0041	0.0070 ± 0.0022	0.0060 ± 0.0025	0.0075 ± 0.0024	0.0177 ± 0.0108
FDB	0.0030 ± 0.0014	0.0031 ± 0.0019	0.0037 ± 0.0030	0.0034 ± 0.0025	0.0213 ± 0.0063	0.0338 ± 0.0260

very strongly to all surfaces irrespective of their degree of hydrophobicity.

The beads containing immobilized CalB were subsequently used for an active-site titration to determine the fraction of enzymes that remained catalytically active after surface adsorption. When CalB reacts with the suicide inhibitor methyl 4-methyl-umbelliferyl hexylphosphonate (ELSI-MF)[46,47] the fluorophore 7-hydroxy-4-methylcoumarin is released in a stoichiometric amount. Consequently, the concentration of 7-hydroxy-4-methylcoumarin corresponds directly to the concentration of active CalB. A comparison of the activity of the immobilized CalB samples with a sample of nonimmobilized CalB shows that 54−70% of enzymes retain their activity upon immobilization on the different surfaces (Table 2). The lowest fraction of active enzymes (54%) was detected on the PEGylated surface. Even though the difference between the surfaces is small, a trend can be observed. The fraction of active enzymes increases with increasing hydrophobicity before it decreases again. The highest fraction of active enzymes was detected on the octyl-terminated surface. This result suggests that there is an optimum hydrophobicity of the immobilization support: at low hydrophobicity the enzyme might not adsorb in the active, lid-open conformation; in contrast, the enzyme might unfold on very hydrophobic surfaces.

Activity Measurements. Four different water-soluble substrates were used to measure the activity of immobilized CalB. To test for the influence of the size of the substrate, the three structurally related fluorogenic substrates fluorescein diacetate (FDA), 5,6-carboxyfluorescein diacetate (CFDA), and fluorescein butyrate (FDB) were chosen and compared to the frequently used chromogenic substrate *para*-nitrophenol butyrate (*p*NPB). Whereas *p*NPB is hydrolyzed by CalB very efficiently, the catalytic activity for the fluorogenic substrate CFDA is very low.[45] This large difference in activity is most likely the result of a very bulky alcohol group, which hinders binding of CFDA into the active site. The use of these substrates not only allows for testing for the size of the alcohol group, but also provides a direct spectroscopic readout of the catalytic reaction in real-time.

Progress curves of the enzymatic reaction using 500 nM immobilized enzyme and 10 μM of fluorogenic substrate are shown in Figure S5. The progress curves show a sigmoidal shape typical for the hydrolysis of a fluorogenic substrate with two enzyme-cleavable bonds.[48−51] This two-step reaction, involving an intermediate with different brightness, complicates the kinetic analysis.[51] To circumvent this problem, only the first 7% of the intensity data points have been used for calculating the enzymatic rate (see SI for details), corresponding to the first conversion step of the substrate into the intermediate. The enzymatic turnover rates for all substrates and surfaces tested are summarized in Table 3.

When comparing the turnover rate for the frequently used substrate *p*NPB, only small differences in CalB activity were observed between the different surfaces and the control sample containing nonimmobilized, free enzyme. In contrast, the turnover rate drastically changed for the substrate FDB when the enzyme was immobilized on the octyl- or octadecyl-terminated surface. On the octyl-terminated surface the turnover rate increased by a factor of 7 and on the octadecyl-terminated surface by a factor of 11, with a large error in the latter case. This higher error originates from the extremely high hydrophobicity of the octadecyl-functionalized beads, which leads to aggregation. Because of this higher error it is difficult to draw conclusions for the substrates CFDA and FDA where the turnover rate is only increased for CalB immobilized on the octadecyl-functionalized surface (2× increase for CFDA; 4× increase for FDA).

The observed increase in catalytic activity might originate from interfacial activation on the hydrophobic surface for the substrate FDB. Alternatively, the substrate FDB might accumulate on the hydrophobic surface, resulting in an increased local concentration of the substrate. Control experiments investigating the autohydrolysis of the different fluorogenic substrates on propyl- and octyl-functionalized beads minimize this second possibility (see SI for details), indicating that the increased catalytic activity is primarily the result of interfacial activation. Molecular dynamics simulations combined with docking studies were carried out to provide more detailed insight into the structural origin of this interfacial activation, most clearly observed for the substrate FDB.

Molecular Dynamics Simulations. To provide structural insight into the mechanism behind this interfacial activation, we applied a combination of molecular dynamics and docking calculations to determine the effect of a hydrophobic interface on the conformational distribution of CalB. As a first step, we used long time scale replica exchange simulations to map out the conformational distribution and dynamics of CalB in aqueous solution. Consistent with previous simulations,[13,26−28] analysis of the mobility of different residues in CalB throughout the replica exchange simulations illustrates a substantially higher flexibility for the α5 helix and to a smaller extent also for the α10 helix. The other secondary structure elements remain fairly rigid throughout the simulations (see Figure S7).

DOI: 10.1021/acs.biochem.5b00586
Biochemistry 2015, 54, 5969−5979

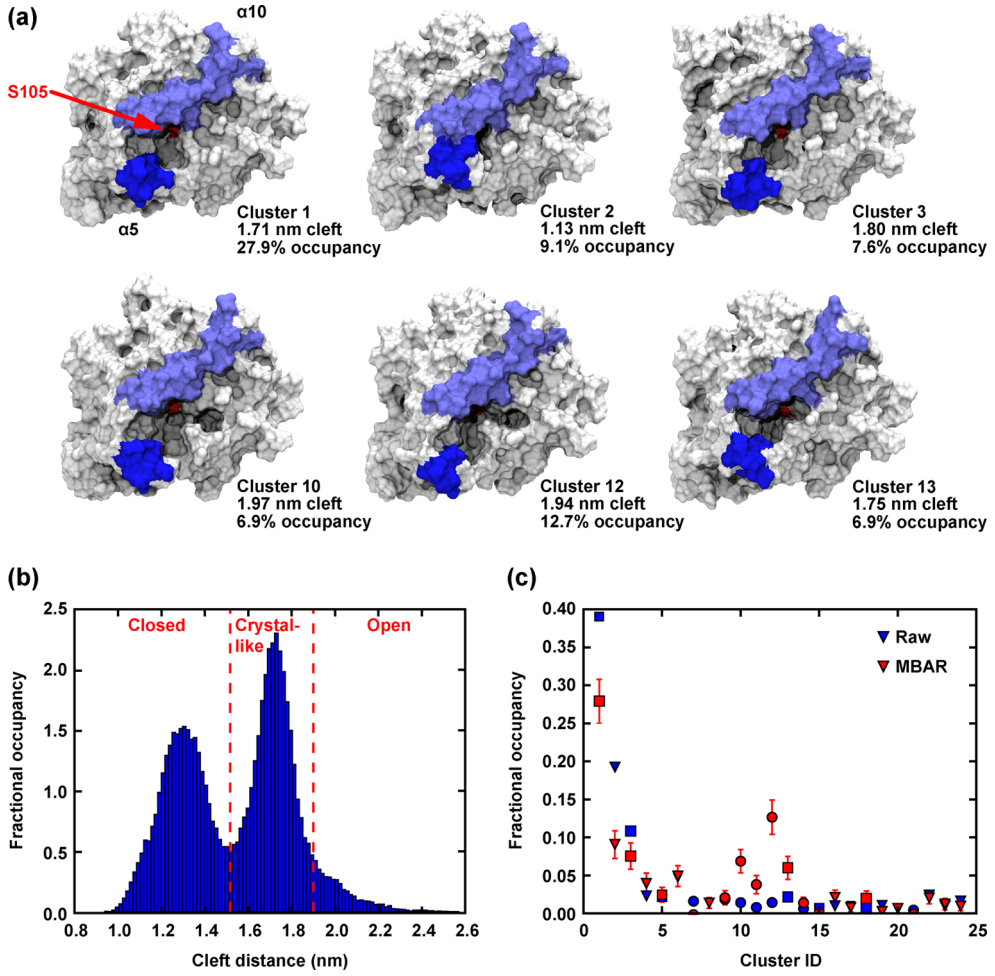

Figure 2. Common conformations of CalB and its active site cleft during replica exchange simulations. (a) Conformations of the six most heavily occupied clusters, including estimated occupancies and width of the active site cleft. (b) Histogram of cleft distances over all replica exchange trajectory frames, illustrating the subdivision of conformations into closed (cleft <1.52 nm, crystal-like, or open states (cleft >1.9 nm). (c) Fractional occupancy of conformational clusters, either calculated from the raw replica exchange trajectories or estimated at 308 K using MBAR.[42] Closed, crystal-like, and open conformations are plotted with triangles, squares, and circles, respectively. Error bars show standard deviations in estimated populations calculated by MBAR.

Clustering analysis (see Experimental Procedures for details) illustrates that the primary conformational change apparent in the trajectories is switching between cleft-closed and cleft-open states of the α5 helix, altering the accessibility of the CalB active site (Figure 2). The conformations of the active site can be subdivided into three categories based on the width of the active site cleft (Figure 2b): closed (cleft width <1.52 nm), crystal-like (1.52−1.9 nm cleft, roughly matching that in the crystal structure), and open (>1.9 nm cleft). Reweighting of the observed conformations by applying the MBAR method to the replica exchange trajectories indicates that at 308 K, the occupancies of clusters falling into these states are 36.1%, 55.6%, and 8.2% for the closed, crystal-like, and open states, respectively.

While kinetic parameters are particularly difficult to estimate from replica exchange simulations due to the changing temperatures, we estimated the approximate lifetimes of different states (closed, crystal-like, open) by monitoring the trajectories of cleft distance vs time. Only stretches of the simulation after the first 6 ns of each replica trajectory, for which the target temperature never rose above 350 K, were considered in the lifetime calculations. Median dwell times in all three major conformations were 20−30 ps for each trajectory, and median times for transition from the closed to open or open to closed state were 2.2 and 5.7 ns, respectively; however, these figures likely underestimate the true dwell times in each conformation because longer dwell times are censored since the temperature at some point rises above the 350 K threshold.

Docking Studies. Our observation that the width of the CalB active site is highly variable provides a possible explanation for the experimental observation that bulkier substrates show qualitatively different behavior in the presence of hydrophobic interfaces. In order to determine whether the conformational state of CalB determines substrate binding, we docked all substrates (Figure S1) to a substrate-analogue bound CalB crystal structure (PDB code 1LBS), to the equilibrated starting structure for the molecular dynamics simulation, and to one representative conformation of each of the 24 most heavily occupied clusters identified by clustering analysis.

Plots of the DOCK binding energies versus cleft distance are shown for all substrates in Figure 3. Two striking patterns emerge from these plots: (i) a marked depletion of favorable conformations with a small cleft distance is observed for the bulkier substrates. In contrast, many closed conformations are able to bind *p*NPB with a low relative binding energy. (ii) FDB

DOI: 10.1021/acs.biochem.5b00586
Biochemistry 2015, 54, 5969−5979

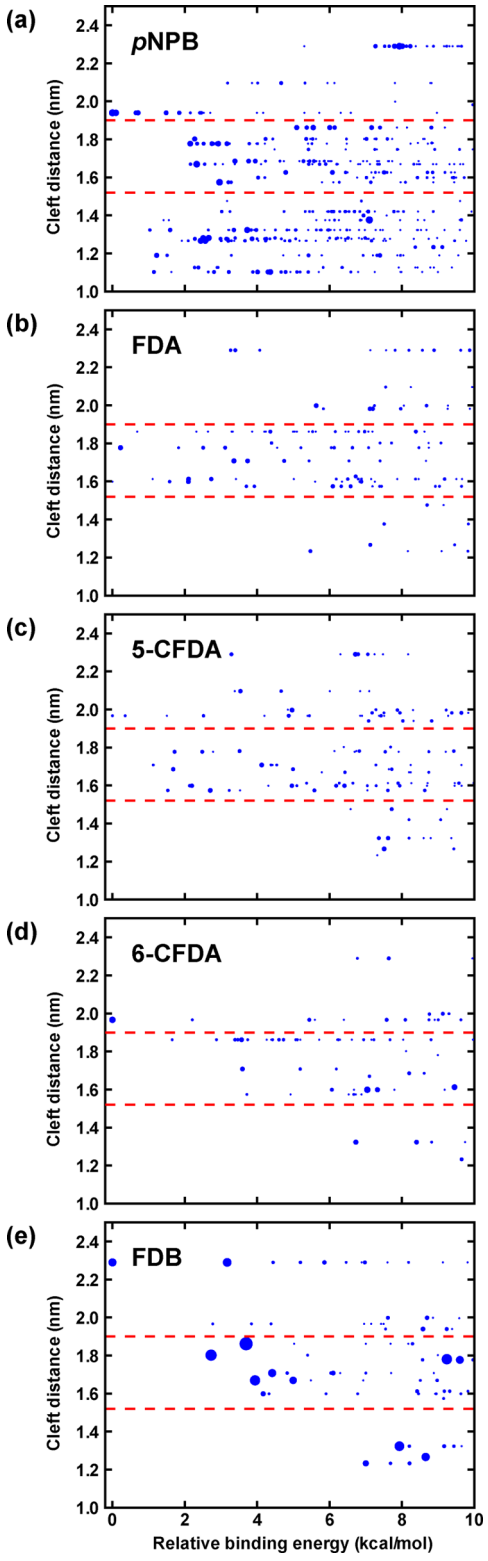

Figure 3. (a–e) DOCK grid score-based binding energies for the docked conformations of all substrates, plotted against the cleft distance of the corresponding protein conformation. The size of each point is proportional to the number of effectively identical docked poses identified (<0.1 nm RMSD). Only catalytically competent conformations are considered (i.e., the distance between the substrate ester carbon and the oxygen of S105 is less than 0.6 nm). Red dashed lines indicate the cleft distance thresholds between the closed, crystal-like and open conformations.

stands unique among all substrates in that its most favorable docked poses correspond to a low-occupancy, highly open cluster (cluster 14, with a cleft distance of 2.29 nm and an estimated fractional occupancy of 0.014 at 308 K).

A comparison of the crystal structure with cluster 14 shows that the mobile α5 helix unfolds completely and leaves the vicinity of the active site cleft (Figure 4a). Figure 4b shows the

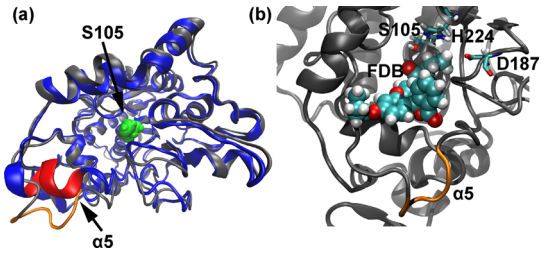

Figure 4. Comparison of a representative cluster 14 conformation with the CalB crystal structure (PDB code 1LBS). (a) The backbone trace of the crystal structure is shown blue; the structure of cluster 14 is shown in gray. The α5 helix is labeled in red (crystal) or orange (cluster 14). The catalytic serine (S105) is highlighted in green. (b) Most favorable, catalytically competent, docked conformation of FDB, showing the location of the substrate, the catalytic triad residues, and the α5 helix (orange).

single best-binding conformation of FDB in cluster 14. This binding pose would be sterically forbidden in the crystal structure due to the conformation of α5. Other favorable binding poses for FDB also correspond to more open conformations, and the closed conformations are particularly disfavored. Comparisons of the best scoring docked poses for all substrates are shown in Figure S8.

Conformational Free Energy Estimates. As discussed above, our experimental data indicate that CalB shows preferential activation toward bulky substrates (in particular FDB) in the presence of a hydrophobic interface. More importantly, the degree of activation increases with interface thickness and consequently hydrophobicity. To provide a molecular-level interpretation for these results, we applied a simplified model to estimate the effect of a hydrophobic layer of varying thickness on the conformational distribution of CalB. This model approximates the silane-functionalized beads as consisting of hydrophobic slab that covers a hydrophilic, impenetrable slab. For each CalB conformation, the protein is treated as a rigid body. We approximated the partition function for the protein in contact with the hydrophobic slab (including all possible orientations and depths; see Figure 5a) using a simplified energy function that is based on the solvent exposed surface area of hydrophilic and hydrophobic side chains. Comparing the partition weights of different conformations allows for an approximation of the relative occupancies of different conformations in the presence of different slab thicknesses.

According to the model, the presence of the hydrophobic slab strongly favors open enzyme conformations (Figure 5b), except for very thin slabs (~0.5 nm). This preference for open enzyme conformations becomes more apparent with increasing slab thicknesses up to approximately 1.5 nm. The reason for this depth dependence is readily apparent from plots of the preferred insertion depths of the different conformations (Figure S9a–c). Whereas most closed conformations do not insert more than 0.4 nm into the hydrophobic slabs, most

DOI: 10.1021/acs.biochem.5b00586
Biochemistry 2015, 54, 5969–5979

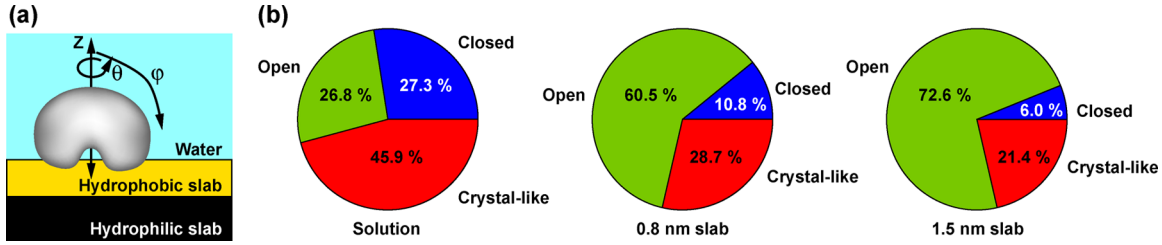

Figure 5. Effects of a hydrophobic interface on cluster occupancy. (a) Schematic of the model used to estimate the effects of a hydrophobic slab. For each cluster, the partition function was approximated on a grid of orientations (θ, φ) and penetration depths (z) of the protein into the hydrophobic slab. The hydrophobic slab represents the silane coating of the glass bead, whereas the bead surface itself was treated as a second, impenetrable hydrophilic slab below the hydrophobic layer. (b) Estimated occupancies of different conformational states of CalB while in contact with a hydrophobic slab of varying thickness.

crystal-like and open conformations favor insertion depths up to 1 nm. It is also notable that all open and crystal-like conformations favor orientations where the active site is buried deeply in the hydrophobic slab. In contrast, the closed state tends to tilt further away from such an alignment (Figure S9d).

Clearly, these low-resolution calculations, designed to test the effect of a hydrophobic interface on the conformational distribution of CalB, suggest that a hydrophobic interface biases the enzyme toward α5-open conformations. These conformations are oriented such that the active site is facing toward the hydrophobic interface so that they are most likely stabilized by the interface. Assuming that the enzyme binds to the surface in the same orientation under experimental conditions, these calculation results directly explain the observed interfacial activation for bulkier substrates and the observed dependence on alkyl chain length (i.e., layer thickness).

DISCUSSION

The activity measurements performed in this study show that the turnover rate of CalB increases when immobilized on surfaces of increasing hydrophobicity. For fluorescein dibutyrate (FDB), which is the fluorogenic substrate with the longest alkyl chain, CalB activity increased 7-fold after immobilization onto the octyl-functionalized surfaces and 11-fold on the octadecyl-functionalized surface. An increased turnover rate was also detected for the other fluorogenic substrates fluorescein diacetate (FDA; 4× increase) and 5,6-carboxyfluorescein diacetate (CFDA; 2× increase), but to a much smaller extent and only on the octadecyl-functionalized surface. In contrast, the turnover rate is not affected by the type of surface when activity is measured with the frequently used chromogenic substrate *para*-nitrophenyl butyrate (*p*NPB), which has a much smaller alcohol substituent than the fluorogenic substrates.

The observed increase in CalB activity for the large, bulky substrates might be caused by a better access of these substrates to the active site on the more hydrophobic surfaces or a conformational change leading to interfacial activation. It has been shown for other lipases that substrate accumulation at the interface leads to a higher local substrate concentration and therefore increased activity.[52−54] We are not able to fully rule out this possibility, but consider it as very unlikely. No differences in product accumulation were observed when substrate autohydrolysis was observed in the vicinity of the functionalized beads (Figure S6). Moreover, the only parts of the substrate that can possibly interact with the alkyl chains coupled to the beads are the substrate alkyl chains. If this was the case, an increased turnover rate should also be observed for *p*NPB hydrolysis, which is not the case. This leads to the conclusion that the increased activity observed on the most hydrophobic surface is indeed the result of a conformational change that improves the access of large, bulky substrates to the active site. This conclusion is strongly supported by the presented simulations, which show that the α5 helix samples a large range of conformations with open conformations being more likely in a hydrophobic environment (Figure 5b).

Interfacial activation is usually observed for most other lipases when their activity is measured in the presence of detergent micelles or any other hydrophobic interface.[1,7] Only a limited number of experiments point to the existence of interfacial activation for CalB under similar experimental conditions, and from these studies no clear conclusions could be drawn. Earlier experiments, in which CalB was immobilized on agarose beads functionalized with octyl chains[52] or Sepabeads functionalized with octadecyl chains,[55] suggested activation effects much smaller than those observed in the present study. Stronger activation was detected for CalB adsorbed on alkyl-terminated self-assembled monolayers on gold.[31] No active site titration was performed, however, and the authors explained the effect with a higher number of active enzymes on the surface. Combining the results of these existing studies with the results obtained here suggests that strong activation is only achieved when CalB adsorbs on a highly packed, self-assembled monolayer of uniform molecular arrangement formed, for example, on gold or using silanization. Clearly, the quality of the hydrophobic interface is crucial for the activation of CalB. It is therefore not unexpected that interfacial activation has hardly been observed before when CalB was immobilized onto alkyl-functionalized polymeric beads where the alkyl chains are less ordered. In addition, these assays have mostly been performed with substrates of smaller size where the cleft opening is less important. It is clearly an interesting topic for future studies to investigate if the immobilization conditions found here will also yield interfacially activated CalB when using other bulky substrates that are not fully water-soluble, but need to be solubilized with detergents or dissolved in organic solvents.

Helix α5 plays a crucial role in the observed activation. This helix has been discussed as a potential lid ever since the crystal structure of CalB has been resolved.[9] As no interfacial activation could be confirmed,[29] however, its role as a lid was questioned later.[13,27,30] Instead it was suggested that α5 acts as an anchor for establishing the initial contact of the enzyme with a hydrophobic interface[27] and that it plays a role in substrate binding.[13] Our simulations confirm that α5 is the most mobile part of the enzyme structure and that it can adopt a large range of different conformations, including transient unfolding

DOI: 10.1021/acs.biochem.5b00586
Biochemistry 2015, 54, 5969−5979

(Figure 4). The conformation of α5 directly determines the cleft distance and therefore the maximum size of the substrate that can fit into the active site. Most importantly, the simulation results show that the open conformations are more frequently occupied when the enzyme is in contact with a hydrophobic interface. Taken together, these simulation results highlight the crucial role of α5 in determining substrate access to the active site and establish that its conformation is regulated by the hydrophobicity of its environment. The simulations do not only show a range of open conformations, but also a number of structures where α5 is more closed than in the crystal structure. In none of these conformations, however, is the active site fully shielded from the solvent: a narrow, open channel remains along with sufficient room in the active site to possibly accommodate small substrates (Figure 3e). In this context, CalB can be considered as an intermediate enzyme acting as an esterase for small substrates with easy access to the active site (e.g., *p*NPB hydrolysis) and as a lipase for larger/bulkier substrates where full access to the active site depends on the structural conformation of the α5 lid. This intermediate status of CalB has already been proposed in 1994 when the crystal structure was published;[9] however, our results are the first experimental proof that CalB does indeed show this behavior. We note that, as all simulations were performed in aqueous solution, the possibility exists that other conformations of the enzyme would also arise in the presence of a hydrophobic layer. The extensive sampling performed here (over one microsecond of simulation, with sampling enhanced by parallel tempering calculations), and the rapid interconversion between closed and open conformations, argue against this possibility but do not exclude it. Given that the closed conformations that we identified almost uniformly disfavored deep insertion into hydrophobic layers, it is still highly likely that any unsampled conformations favored by a hydrophobic environment would most likely resemble open state conformations as we describe above.

In conclusion, the results obtained from our combined experimental and simulation approach point toward the existence of an atypical interfacial activation of CalB on highly hydrophobic supports when the enzyme hydrolyzes large/bulky substrates. It is difficult to conclude if this regulation of substrate specificity and catalytic activity is of importance for the natural function of CalB, as its natural substrate is not known. One can easily imagine that this is an elegant way of making use of one and the same enzyme for different functions in the native environment. More importantly, this information about the crucial role of the α5 helix provides a new starting point for the optimization of CalB for industrial applications. Our results provide clear evidence that CalB possesses a larger, more open active site when immobilized on a well-packed, hydrophobic surface. It might, therefore, be able to accommodate a larger range of substrates with bulkier and aromatic alcohol substituents that are usually not hydrolyzed efficiently.

■ ASSOCIATED CONTENT

Supporting Information

The Supporting Information is available free of charge on the ACS Publications website at DOI: 10.1021/acs.biochem.5b00586.

Detailed methods for the expression, purification and labeling of CalB as well as for the characterization of the silanized surfaces; detailed information about the calculation of the enzymatic rate as well as additional simulation results (PDF)

■ AUTHOR INFORMATION

Corresponding Authors

*(A.E.R.) E-mail: a.rowan@science.ru.nl.

*(K.G.B.) Present address: Max Planck Institute of Colloids and Interfaces, Mechano(bio)chemistry, Potsdam-Golm Science Park, 14424 Potsdam, Germany. E-mail: kerstin.blank@mpikg.mpg.de.

Present Address

#(M.C.F.v.T.) Radboud University, Microbiology, Heyendaalseweg 135, 6525 AJ Nijmegen, The Netherlands.

Funding

This work was supported by the Dutch National Research School Combination Catalysis Controlled by Chemical Design (NRSCC Grant 2009-10016B, A.E.R.), The Netherlands Organisation for Scientific Research (NWO; VIDI Grant 700.58.430, K.B.; Gravitation Program 024.001.035), and the United States National Institutes of Health (NIH K99/R00GM097033, P.L.F.). Computer time was provided by an XSEDE Grant TG-MCA05S028 to Klaus Schulten (University of Illinois at Urbana-Champaign).

Notes

The authors declare no competing financial interest.

■ ACKNOWLEDGMENTS

We gratefully acknowledge Klaus Schulten for providing computer time for this project and Laura Cattaneo for help with characterizing the silanized surfaces.

■ REFERENCES

(1) Verger, R. (1997) 'Interfacial activation' of lipases: Facts and artifacts. *Trends Biotechnol. 15*, 32−38.

(2) Fojan, P., Jonson, P. H., Petersen, M. T. N., and Petersen, S. B. (2000) What distinguishes an esterase from a lipase: A novel structural approach. *Biochimie 82*, 1033−1041.

(3) Reis, P., Holmberg, K., Watzke, H., Leser, M. E., and Miller, R. (2009) Lipases at interfaces: A review. *Adv. Colloid Interface Sci. 147−148*, 237−250.

(4) Ghanem, A. (2007) Trends in lipase-catalyzed asymmetric access to enantiomerically pure/enriched compounds. *Tetrahedron 63*, 1721−1754.

(5) Brzozowski, A. M., Derewenda, U., Derewenda, Z. S., Dodson, G. G., Lawson, D. M., Turkenburg, J. P., Bjorkling, F., Huge-Jensen, B., Patkar, S. A., and Thim, L. (1991) A model for interfacial activation in lipases from the structure of a fungal lipase-inhibitor complex. *Nature 351*, 491−494.

(6) Derewenda, U., Brzozowski, A. M., Lawson, D. M., and Derewenda, Z. S. (1992) Catalysis at the interface: the anatomy of a conformational change in a triglyceride lipase. *Biochemistry 31*, 1532−1541.

(7) Schmid, R. D., and Verger, R. (1998) Lipases: Interfacial Enzymes with Attractive Applications. *Angew. Chem., Int. Ed. 37*, 1608−1633.

(8) Adlercreutz, P. (2013) Immobilisation and application of lipases in organic media. *Chem. Soc. Rev. 42*, 6406−6436.

(9) Uppenberg, J., Hansen, M. T., Patkar, S., and Jones, T. A. (1994) The sequence, crystal structure determination and refinement of two crystal forms of lipase B from *Candida antarctica*. *Structure 2*, 293−308.

(10) Uppenberg, J., Oehrner, N., Norin, M., Hult, K., Kleywegt, G. J., Patkar, S., Waagen, V., Anthonsen, T., and Jones, T. A. (1995) Crystallographic and molecular-modeling studies of lipase B from

DOI: 10.1021/acs.biochem.5b00586
Biochemistry 2015, 54, 5969−5979

Candida antarctica reveal a stereospecificity pocket for secondary alcohols. *Biochemistry 34*, 16838−16851.
(11) Morita, T., Koike, H., Koyama, Y., Hagiwara, H., Ito, E., Fukuoka, T., Imura, T., Machida, M., and Kitamoto, D. (2013) Genome Sequence of the Basidiomycetous Yeast *Pseudozyma antarctica* T-34, a Producer of the Glycolipid Biosurfactants Mannosylerythritol Lipids. *Genome Announc. 1*, e0006413.
(12) Anderson, E. M., Larsson, K. M., and Kirk, O. (1998) One biocatalyst - many applications: The use of *Candida antarctica* B-Lipase in organic synthesis. *Biocatal. Biotransform. 16*, 181−204.
(13) Skjøt, M., De Maria, L., Chatterjee, R., Svendsen, A., Patkar, S. A., Østergaard, P. R., and Brask, J. (2009) Understanding the Plasticity of the α/β Hydrolase Fold: Lid Swapping on the *Candida antarctica* Lipase B Results in Chimeras with Interesting Biocatalytic Properties. *ChemBioChem 10*, 520−527.
(14) Palomo, J. M., Fernández-Lorente, G., Mateo, C., Fuentes, M., Fernández-Lafuente, R., and Guisan, J. M. (2002) Modulation of the enantioselectivity of *Candida antarctica* B lipase via conformational engineering. Kinetic resolution of (±)-α-hydroxy-phenylacetic acid derivatives. *Tetrahedron: Asymmetry 13*, 1337−1345.
(15) Fernandez-Lorente, G., Cabrera, Z., Godoy, C., Fernandez-Lafuente, R., Palomo, J. M., and Guisan, J. M. (2008) Interfacially activated lipases against hydrophobic supports: Effect of the support nature on the biocatalytic properties. *Process Biochem. 43*, 1061−1067.
(16) Cabrera, Z., Fernandez-Lorente, G., Fernandez-Lafuente, R., Palomo, J. M., and Guisan, J. M. (2009) Novozym 435 displays very different selectivity compared to lipase from *Candida antarctica* B adsorbed on other hydrophobic supports. *J. Mol. Catal. B: Enzym. 57*, 171−176.
(17) Orrenius, C., Hæffner, F., Rotticci, D., Öhrner, N., Norin, T., and Hult, K. (1998) Chiral Recognition Of Alcohol Enantiomers In Acyl Transfer Reactions Catalysed By *Candida antarctica* Lipase B. *Biocatal. Biotransform. 16*, 1−15.
(18) Ottosson, J., Rotticci-Mulder, J. C., Rotticci, D., and Hult, K. (2001) Rational design of enantioselective enzymes requires considerations of entropy. *Protein Sci. 10*, 1769−1774.
(19) Magnusson, A. O., Rotticci-Mulder, J. C., Santagostino, A., and Hult, K. (2005) Creating Space for Large Secondary Alcohols by Rational Redesign of *Candida antarctica* Lipase B. *ChemBioChem 6*, 1051−1056.
(20) Magnusson, A. O., Takwa, M., Hamberg, A., and Hult, K. (2005) An S-Selective Lipase Was Created by Rational Redesign and the Enantioselectivity Increased with Temperature. *Angew. Chem., Int. Ed. 44*, 4582−4585.
(21) Liu, D., Trodler, P., Eiben, S., Koschorreck, K., Müller, M., Pleiss, J., Maurer, S. C., Branneby, C., Schmid, R. D., and Hauer, B. (2010) Rational design of *Pseudozyma antarctica* lipase B yielding a general esterification catalyst. *ChemBioChem 11*, 789−795.
(22) Juhl, P. B., Doderer, K., Hollmann, F., Thum, O., and Pleiss, J. (2010) Engineering of *Candida antarctica* lipase B for hydrolysis of bulky carboxylic acid esters. *J. Biotechnol. 150*, 474−480.
(23) Qian, Z., and Lutz, S. (2005) Improving the catalytic activity of *Candida antarctica* lipase B by circular permutation. *J. Am. Chem. Soc. 127*, 13466−13467.
(24) Qian, Z., Fields, C. J., and Lutz, S. (2007) Investigating the Structural and Functional Consequences of Circular Permutation on Lipase B from *Candida antarctica*. *ChemBioChem 8*, 1989−1996.
(25) Gumpp, H., Puchner, E. M., Zimmermann, J. L., Gerland, U., Gaub, H. E., and Blank, K. (2009) Triggering enzymatic activity with force. *Nano Lett. 9*, 3290−3295.
(26) Kumaresan, J., Kothai, T., and Lakshmi, B. S. (2011) In silico approaches towards understanding CALB using molecular dynamics simulation and docking. *Mol. Simul. 37*, 1053−1061.
(27) Gruber, C. C., and Pleiss, J. (2012) Lipase B from *Candida antarctica* binds to hydrophobic substrate−water interfaces via hydrophobic anchors surrounding the active site entrance. *J. Mol. Catal. B: Enzym. 84*, 48−54.
(28) Irani, M., Törnvall, U., Genheden, S., Larsen, M. W., Hatti-Kaul, R., and Ryde, U. (2013) Amino acid oxidation of *Candida antarctica* lipase B studied by molecular dynamics simulations and site-directed mutagenesis. *Biochemistry 52*, 1280−1289.
(29) Martinelle, M., Holmquist, M., and Hult, K. (1995) On the interfacial activation of *Candida antarctica* lipase A and B as compared with *Humicola lanuginosa* lipase. *Biochim. Biophys. Acta, Lipids Lipid Metab. 1258*, 272−276.
(30) Overbeeke, P. L. A., Govardhan, C., Khalaf, N., Jongejan, J. A., and Heijnen, J. J. (2000) Influence of lid conformation on lipase enantioselectivity. *J. Mol. Catal. B: Enzym. 10*, 385−393.
(31) Laszlo, J. A., and Evans, K. O. (2007) Influence of self-assembled monolayer surface chemistry on *Candida antarctica* lipase B adsorption and specific activity. *J. Mol. Catal. B: Enzym. 48*, 84−89.
(32) Phillips, J. C., Braun, R., Wang, W., Gumbart, J., Tajkhorshid, E., Villa, E., Chipot, C., Skeel, R. D., Kalé, L., and Schulten, K. (2005) Scalable molecular dynamics with NAMD. *J. Comput. Chem. 26*, 1781−1802.
(33) MacKerell, A. D., Brooks, B., Brooks, C. L., Nilsson, L., Roux, B., Won, Y., and Karplus, M. (1998) CHARMM: The Energy Function and Its Parameterization with an Overview of the Program, in *The Encyclopedia of Computational Chemistry*, pp 271−277, John Wiley & Sons, Chichester.
(34) MacKerell, A. D., Feig, M., and Brooks, C. L. (2004) Extending the treatment of backbone energetics in protein force fields: Limitations of gas-phase quantum mechanics in reproducing protein conformational distributions in molecular dynamics simulations. *J. Comput. Chem. 25*, 1400−1415.
(35) Jorgensen, W. L., Chandrasekhar, J., Madura, J. D., Impey, R. W., and Klein, M. L. (1983) Comparison of simple potential functions for simulating liquid water. *J. Chem. Phys. 79*, 926−935.
(36) Humphrey, W., Dalke, A., and Schulten, K. (1996) VMD: Visual Molecular Dynamics. *J. Mol. Graphics 14*, 33−38.
(37) Sugita, Y., and Okamoto, Y. (1999) Replica-exchange molecular dynamics method for protein folding. *Chem. Phys. Lett. 314*, 141−151.
(38) Van Der Spoel, D., Lindahl, E., Hess, B., Groenhof, G., Mark, A. E., and Berendsen, H. J. C. (2005) GROMACS: Fast, flexible, and free. *J. Comput. Chem. 26*, 1701−1718.
(39) Daura, X., Gademann, K., Jaun, B., Seebach, D., van Gunsteren, W. F., and Mark, A. E. (1999) Peptide Folding: When Simulation Meets Experiment. *Angew. Chem., Int. Ed. 38*, 236−240.
(40) Pettersen, E. F., Goddard, T. D., Huang, C. C., Couch, G. S., Greenblatt, D. M., Meng, E. C., and Ferrin, T. E. (2004) UCSF Chimera - a visualization system for exploratory research and analysis. *J. Comput. Chem. 25*, 1605−1612.
(41) Lang, P. T., Moustakas, D., Brozell, S., Carrascal, N., Mukherjee, S., Balius, T., Allen, W. J., Holden, P., Pegg, S., Raha, K., Shivakumar, D., Rizzo, R., Case, D., Shoichet, B., and Kuntz, I. (2006) *DOCK 6.1 Users Manual*.
(42) Shirts, M. R., and Chodera, J. D. (2008) Statistically optimal analysis of samples from multiple equilibrium states. *J. Chem. Phys. 129*, 124105.
(43) Radzicka, A., and Wolfenden, R. (1988) Comparing the Polarities of the Amino Acids: Side Chain Distribution Coefficients between the Vapor Phase, Cyclohexane, 1-Octanol, and Neutral Aqueous Solution. *Biochemistry 27*, 1664−1670.
(44) Blank, K., Morfill, J., and Gaub, H. E. (2006) Site-specific immobilization of genetically engineered variants of *Candida antarctica* lipase B. *ChemBioChem 7*, 1349−1351.
(45) Blank, K., Morfill, J., Gumpp, H., and Gaub, H. E. (2006) Functional expression of *Candida antarctica* lipase B in Escherichia coli. *J. Biotechnol. 125*, 474−483.
(46) Rotticci, D., Norin, T., Hult, K., and Martinelle, M. (2000) An active-site titration method for lipases. *Biochim. Biophys. Acta, Mol. Cell Biol. Lipids 1483*, 132−140.
(47) Fujii, R., Utsunomiya, Y., Hiratake, J., Sogabe, A., and Sakata, K. (2003) Highly sensitive active-site titration of lipase in microscale culture media using fluorescent organophosphorus ester. *Biochim. Biophys. Acta, Mol. Cell Biol. Lipids 1631*, 197−205.

DOI: 10.1021/acs.biochem.5b00586
Biochemistry 2015, 54, 5969−5979

(48) Hofmann, J., and Sernetz, M. (1983) A kinetic study on the enzymatic hydrolysis of fluorescein diacetate and fluorescein-di-beta-D-galactopyranoside. *Anal. Biochem. 131*, 180−186.
(49) Huang, Z. J. (1991) Kinetic fluorescence measurement of fluorescein di-beta-D-galactoside hydrolysis by beta-galactosidase: intermediate channeling in stepwise catalysis by a free single enzyme. *Biochemistry 30*, 8535−8540.
(50) Fiedler, F., and Hinz, H. (1994) No intermediate channelling in stepwise hydrolysis of fluorescein di-β-D-galactoside by β-galactosidase. *Eur. J. Biochem. 222*, 75−81.
(51) Terentyeva, T. G., Van Rossom, W., Van der Auweraer, M., Blank, K., and Hofkens, J. (2011) Morpholinecarbonyl-Rhodamine 110 based substrates for the determination of protease activity with accurate kinetic parameters. *Bioconjugate Chem. 22*, 1932−1938.
(52) Fernandez-Lafuente, R., Armisén, P., Sabuquillo, P., Fernández-Lorente, G., and Guisán, J. M. (1998) Immobilization of lipases by selective adsorption on hydrophobic supports. *Chem. Phys. Lipids 93*, 185−197.
(53) Rotticci, D., Norin, T., and Hult, K. (2000) Mass Transport Limitations Reduce the Effective Stereospecificity in Enzyme-Catalyzed Kinetic Resolution. *Org. Lett. 2*, 1373−1376.
(54) Fernández-Lorente, G., Palomo, J. M., Cabrera, Z., Guisán, J. M., and Fernández-Lafuente, R. (2007) Specificity enhancement towards hydrophobic substrates by immobilization of lipases by interfacial activation on hydrophobic supports. *Enzyme Microb. Technol. 41*, 565−569.
(55) Palomo, J. M., Muñoz, G., Fernández-Lorente, G., Mateo, C., Fernández-Lafuente, R., and Guisán, J. M. (2002) Interfacial adsorption of lipases on very hydrophobic support (octadecyl−Sepabeads): immobilization, hyperactivation and stabilization of the open form of lipases. *J. Mol. Catal. B: Enzym. 19−20*, 279−286.

DOI: 10.1021/acs.biochem.5b00586
Biochemistry 2015, 54, 5969−5979